

Functional Imaging to Understand Biomechanics: A Critical Tool for the Study of Biology, Pathology and the Development of Pharmacological Solutions

R. Aidan Jamison^{1,2}, James A. Armitage³, Josie Carberry², Marcus J. Kitchen⁴, Stuart B. Hooper⁵, and Andreas Fouras^{1,*}

¹Division of Biological Engineering, Monash University, Victoria 3800, Australia; ²Department of Mechanical and Aerospace Engineering, Monash University, Victoria 3800, Australia; ³Department of Anatomy and Developmental Biology, Monash University, Victoria 3800, Australia; ⁴School of Physics, Monash University, Victoria 3800, Australia; ⁵The Ritchie Centre, Monash Institute for Medical Research, Monash University, Victoria 3800, Australia

Abstract: We present four case studies of the literature discussing the effects of physical forces on biological function. While the field of biomechanics has existed for many decades, it may be considered by some a poor cousin to biochemistry and other traditional fields of medical research. In these case studies, including cardiovascular and respiratory systems, we demonstrate that, in fact, many systems historically believed to be controlled by biochemistry are dominated by biomechanics. We discuss both the previous paradigms that have advanced research in these fields and the changing paradigms that will define the progressions of these fields for decades to come. In the case of biomechanical effects of flowing blood on the endothelium, this has been well understood for decades. In the cases of platelet activation and liquid clearance from the lungs during birth, these discoveries are far more recent and perhaps not as universally accepted. While only a few specific examples are examined here, it is clear that not enough attention is paid to the possible mechanical links to biological function. The continued development of these research areas, with the inclusion of physical effects, will hopefully provide new insight into disease development, progression, diagnosis and effective therapies.

Keywords: Biomechanics, lung mechanics, cell mechanics, function, functional imaging.

1. INTRODUCTION

Since the development of modern medicine, physicians and researchers have been searching for cures and preventative measures for all diseases that affect mankind. The progression of modern medicine has seen human life expectancies rise greatly over the past century. Although vaccines and living conditions are helping those in the developed world live longer, we are now identifying diseases related to lifestyle choices and wear and tear as the key causes of death. Arterial diseases, such as atherosclerosis, are now the leading cause of death and morbidity in the developed world. Furthermore, the United States Centres for Disease Control and Prevention has declared diabetes an epidemic and diabetes is the fastest growing chronic disease [1].

Although the theory that physical forces play a role on biological function has been studied for many decades, few researchers have chosen to investigate its effect. This is due to the overwhelming support for more traditionally investigated areas, such as biochemistry and pharmacology. This should not come as a surprise as the appeal of understanding the pharmacological mechanisms is clear as it immediately creates a pathway for treatment. As a counter

example, determining the shear stress on the walls of an aneurysm does not immediately provide a solution to the formation or progression of aneurysms [2]. However, understanding the physical forces involved helps to predict the likely progression, and thus would provide an invaluable tool in the decision for surgical intervention. Indeed, investigating shear forces on platelets has recently found that platelet aggregation is controlled by shear forces experienced by the platelet [3]. As the shear forces affect the platelet through a chemical pathway this allows pharmacological treatment for a physically mediated effect. In recent years the interest in the physical forces present within biological systems has dramatically increased with the realisation that choosing to neglect the effect of these forces cannot provide complete explanations for many biological functions. In addition, increasing capacity for functional imaging is making this task simpler and easier [4]. This review is in no means a complete study of the vast field of biomechanics. It, however, focuses on four example areas in which physical forces are emerging as the primary instigator in biological function and that are advancing due to recent developments in functional imaging.

This paper begins with a review of endothelial cell research and the development of identifying shear stress as a key factor in regards to vessel wall health (Section 2). We begin with this example because these discoveries date back over half a century and are now well accepted. Section 3 continues with a discussion on the clearance of lungs

*Address correspondence to this author at the Division of Biological Engineering, Monash University, Victoria 3800, Australia; Tel:+61 3 9905 3493; E-mail: andreas.fouras@monash.edu

immediately after birth and the new discoveries revealing that liquid reabsorption alone is incapable of explaining this process. Section 4 provides a summary of platelet adhesion and activation, with key focus on combining currently available techniques to collect measurements capable of providing new insight into this area. Section 5 reviews how the mechanical properties of erythrocytes impact directly upon biological processes and disease. These three sections (3, 4 and 5) discuss newer less established work that have been chosen to span different scales, from μm platelets to lungs at tens of cm. Furthermore, we hope that any reader can relate to at least one of these very diverse physiological systems. Finally, the paper concludes with a summary of the impact the above-mentioned physical effects have on biological function.

2. ENDOTHELIAL CELLS

The idea that haemodynamics was responsible for the development of atherosclerosis was first investigated by Texon [5] over half a century ago. Texon successfully demonstrated that haemodynamics could effectively predict regions susceptible to atherosclerosis, using fluid mechanics theories to link geometries that caused areas of localised low endothelium shear stress (ESS) with areas where plaque development is most commonly found. This paradigm shift, from the biological to the physical, has led to the understanding of atherosclerosis that we have today.

The endothelial cells are the innermost part of a blood vessel, as shown in Fig. (1). They form a thin tissue on the inside of the vessel wall and are a type of epithelium tissue, simple squamous epithelium, which is only one cell thick. As a result they are directly in contact with blood flowing throughout the body and are thus directly subjected to the fluid-based forces that are present. Endothelial tissue acts as a protective barrier to the tissue beneath by using its ability to generate biological effectors [6]. Fluidic forces from blood are transferred to the endothelial cells via shear. The wall shear stress, a commonly used fluid mechanics measurement, is most easily understood as the frictional force exerted by the fluid on the wall, which develops due to fluid viscosity and flow gradients near the wall. Commonly, wall shear stress is referred to as ESS when investigating blood flow *in vivo*, and will be used henceforth.

A novel approach to investigate endothelial cell orientation was devised a decade later by Flaherty *et al.* [7] in which they removed a section of the middle descending thoracic aorta, rotated the segment 90 degrees, and then replaced it. The animals (mongrel dogs) were examined postoperatively and it was found that the endothelial cells in animals with 10 or more days exposure to aortic blood flow had realigned with the longitudinal axis. Davies *et al.* [8] performed a more detailed *in vitro* study regarding endothelial cell alignment, finding that alignment to the direction of flow began after 7-9 hours of unidirectional steady flow. These studies were some of the first to clearly demonstrate the highly dynamic nature of endothelial cells in response to the fluidic forces present within blood vessels.

The periodic nature of the cardiac cycle induces pulsatile ESS in the vasculature, however, it is areas of more complex geometry, such as bends and bifurcations, that the ESS can

be drastically altered. Although low ESS was originally the concept behind haemodynamic influence on atherosclerosis, further investigation determined that areas in which disturbed flow occurred, such as oscillatory ESS, also positively correlated with plaque location [9]. It is now recognised that ESS plays the most fundamental role in atherosclerosis [10, 11], with significant research being put into not only the identification of areas most prone to ESS [12-14] but also the biological result of altered ESS [15-17].

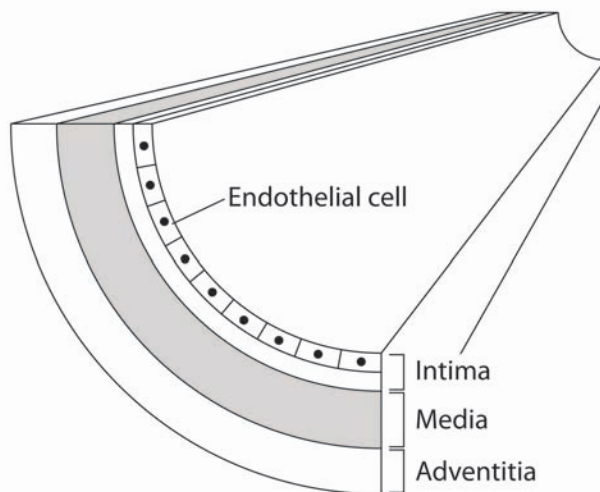


Fig. (1). Schematic section of the wall of a blood vessel.

Endothelial cells are seen to express atheroprotective genes and suppress pro-atherogenic genes in locations of normal flow, however, the opposite is true for areas of disturbed flow [6, 18]. This leads to the initial development of arterial disease, with the progression of arterial disease creating a constantly changing ESS environment, causing dynamic cellular and structural responses [19]. Endothelial cells are capable of being exposed to various types of altered shear stress, of which the three most common are low shear stress, high shear stress and oscillatory shear stress.

The effects of low ESS were initially discussed by Texon [5] and Caro *et al.* [20], with Ku *et al.* [9] providing a detailed investigation comparing wall shear stress in a carotid bifurcation model to plaque locations from cadavers. However, although these studies identified low ESS as correlating positively with plaque location, the cause of the development was still unknown. It is now known that areas of low ESS are atherogenic [21], inducing intimal thickening, attenuating nitric oxide dependent atheroprotection, upregulating vascular endothelial growth factor and enhancing inflammation [10, 16].

Once plaque formation has occurred, located between the endothelial and the outer vessel wall, the arterial wall acts to maintain the original inner caliber of the blood vessel [22]. Under normal ESS conditions compensatory expansive remodelling produces limited inflammation, producing a quiescent plaque, which occurs in ~60% of cases [23]. However, in areas of low ESS, excessive expansive remodelling can occur (~20%), producing intense

inflammation, lowering the ESS further and creating a perpetual cycle. This process leads to a thin cap over the plaque, which is known to have a higher probability of rupture [15]. It is currently thought that the severity of excessive expansive remodelling is significantly associated with the magnitude of low ESS [10].

While areas of low ESS are associated with excessive expansive remodelling, ~20% of cases have constrictive remodelling, in which the narrowing of the blood vessel causes localized areas of high ESS. The local reduction in vessel diameter leads to an increase in velocity due to continuity of mass. This increased velocity creates an increased velocity gradient at the wall, increasing the ESS. As there is no longer a low ESS region the adverse effects leading to the initial development and progression are no longer present, leading to a stable, but stenosed, vessel [23, 24]. However, high ESS is known to cause damage and erosion of endothelial cells and lead to desquamation [17, 25, 26]. The damage or loss of endothelial cells in areas of atherosclerotic plaque formation removes the protective layer between the blood and the plaque itself and can lead to rupture [11, 17].

While low and high ESS have been thoroughly investigated, the effects of oscillatory ESS are generally considered to be similar to low ESS. More recent studies have begun investigating the subtle differences, with Cheng *et al.* [15] developing a unique *in vivo* investigatory technique. Animals (apoE^{-/-} mice) had casts placed around vessels to create various shear conditions; high, low and oscillatory. The mice were then fed an atherogenic diet until humanely killed at different time points (6, 9 and 12 weeks) and the vessels scrutinised. Cheng *et al.* [15] concluded that low ESS creates lesions with a vulnerable phenotype and that oscillatory ESS induces the growth of more stable plaques.

Although the aforementioned studies have all helped assess the shear conditions which cause undesirable ESS, the ability to determine the ESS within humans with high certainty still eludes us. Currently it is possible to combine magnetic resonance imaging (MRI), in order to determine a patient specific geometry, and computational fluid dynamics (CFD), to compute the fluid forces present [27, 28]. However, questions over standard assumptions, such as rigid vessel walls and Newtonian flow [29, 30], require that these simulations still be validated with *in vivo* data wherever possible [31, 32].

The ability to obtain full field blood velocity measurements is essential in developing the capability to diagnose disease *in vivo*. Recent developments in X-ray velocimetry [33-37] are enabling the investigation of whole blood velocities at high spatial and temporal resolution. High resolution velocity measurements allow the accurate calculation of ESS [38]. We have recently demonstrated the ability to measure wall shear stress *in vitro* with physiological flow rates within realistic stenosis models [13]. This study utilises a combination of synchrotron X-ray imaging and particle image velocimetry. Fig. (2) shows an example of the combined velocity and ESS measurements obtained using this technique. Our results were able to identify small variations in ESS along both the stenosed and straight vessel walls throughout the pulsatile cycle.

Additionally, we found that although ESS is generally strongly related to flow rate, that immediately after a stenosis there was no longer a correlation. Additionally, we have developed a limited projection computed tomographic X-ray velocimetry technique, which, if implemented with multiple sources and detectors, could obtain instantaneous 3D velocity measurements [39].

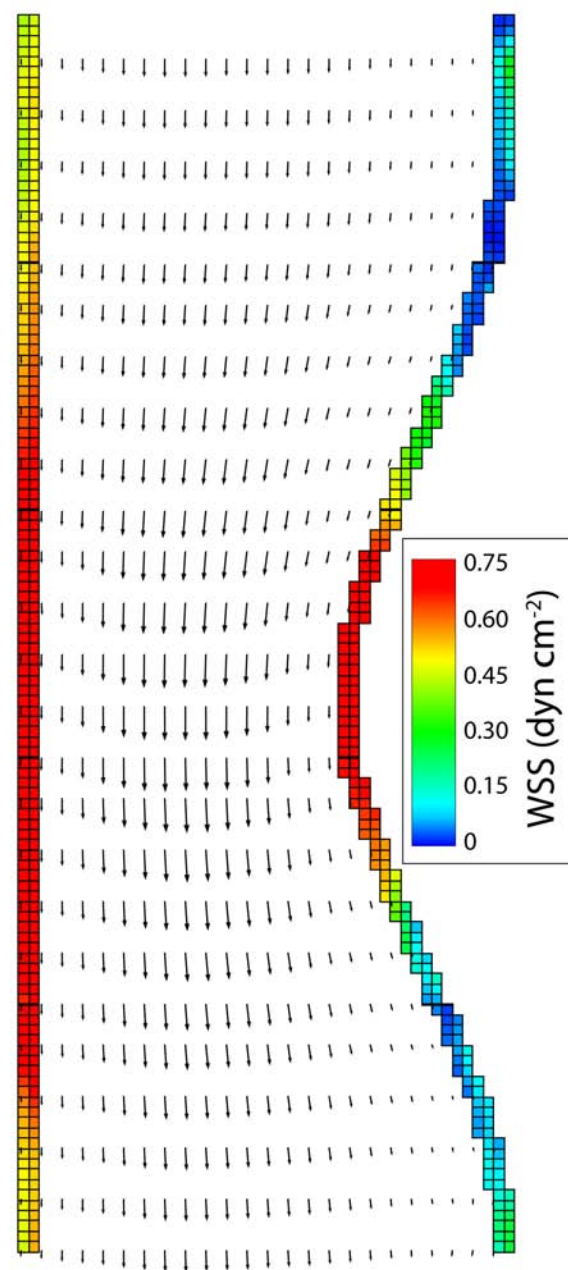


Fig. (2). X-ray velocimetry measurements shown as vectors with the corresponding coloured wall shear stress. Vectors show the direction and magnitude of the flow. For clarity, only every fifth vector is shown in the vertical direction and every second in the horizontal direction. The mesh applied to the wall shear stress illustrates the resolution of the technique. For reference, the narrowest section of the stenosis is 1 mm in diameter.

Although a frontrunner for the most ideal method for the determination of ESS *in vivo* has not yet emerged, development of all techniques will inevitably lead to the most suitable and effective technique for assisting physicians in their daily decisions. This ability would represent a great leap forward in current clinical diagnostic techniques.

3. LUNGS

Of all the organs in the body the lung is amongst the most exposed to physical forces. Lung diseases restrict airflow into or out of the lungs either by increasing airway resistance or by altering lung structure, which in turn changes the elasto-mechanical and aero-resistive properties of the lung [40, 41]. For example, interstitial fibrosis increases distal airway stiffness, asthma increases airway resistance and emphysema reduces lung tissue recoil thereby increasing its compliance. Although these diseases differ markedly in both cause and consequence, they all alter the mechanical properties of diseased regions [42-44]. We have recently shown that the altered mechanical properties of the lung alter the patterns of lung motion which can in turn be used to detect lung disease [Fouras 2011].

Fouras, A., Allison, B. J., Kitchen, M. J., Dubsky, S., Nguyen, J., Hourigan, K., Siu, K.K.W., Lewis, R. A., Wallace, M. J. & Hooper, S. B. Altered lung motion is a sensitive indicator of regional lung disease. *Ann Biomed Eng.* 2011, DOI: 10.1007/s10439-011-0493-0.

It is beyond the scope of this paper to cover all of these varied aspects of lung biomechanics, instead we will focus on the biomechanics of the neonatal lung during birth. One of the greatest challenges to survival faced by a baby following its birth is the transition to air breathing. Respiratory failure at birth is the greatest cause of morbidity and mortality in newborn infants. Before birth, the airways are liquid filled and the fetal lungs take no part in gas exchange, which occurs across the placenta [45, 46]. The airways must be cleared of liquid to enable the entry of air and the establishment of gaseous ventilation.

It is widely accepted that airway liquid clearance and lung aeration are primarily induced by adrenaline-induced activation of epithelial Na⁺ channels (ENaCs), causing Na⁺ reabsorption and reversal of the transepithelial osmotic gradient, leading to water uptake from the airway [47, 48].

However, this is unlikely to be the only mechanism [49], particularly in very preterm infants, since this mechanism matures late in gestation [50-52] and is unlikely to be active in these infants [53]. Mechanical forces imposed on the fetus during labour can also contribute to lung fluid clearance [49, 54]. Although it is unlikely that vaginal squeeze associated with delivery is a major contributing factor [55], the postural changes imposed on the fetus during uterine contractions likely account for the loss of some liquid via the nose and mouth [46, 49]. Increased spinal flexion of the fetus associated with uterine contractions increases fetal abdominal pressure, elevates the diaphragm and increases thoracic pressure, leading to lung liquid loss, particularly following the loss of amniotic fluid volume [56]. The large compliance of the fetal respiratory system in late gestation [57], enables large volumes of lung liquid to be lost shortly after the first signs of labour [58], possibly due to small pressure gradients created by fetal postural changes.

We have recently provided new evidence that challenges existing ideas about lung liquid clearance and aeration at birth. Our results, obtained using phase contrast X-ray imaging (PCXI), suggest that mechanical forces associated with breathing provide the primary mechanism for airway liquid removal [59-61].

Numerous phase contrast imaging modalities abound (see e.g. [62, 63]), all of which require a degree of partial coherence of the X-ray source. We have employed the simplest phase contrast technique, known as propagation-based phase contrast imaging, whereby phase effects are rendered visible by allowing the X-rays that refract (change direction) through an object to propagate away from the source and interfere with the non-refracted X-rays (see paper Snigirev *et al.* [64] for further detail). Hence the interference contrast is largest at the boundaries between where the refractive index gradients are the greatest.

Synchrotrons are capable of producing a bright, partially coherent X-ray beam that is sufficiently large to enable dynamic phase contrast imaging experiments to be performed in near real-time on live animals [65]. Our lung imaging studies [59-62, 65, 66] have been conducted on beamline 20B2 of the worlds largest 3rd generation synchrotron, SPring-8, Japan.

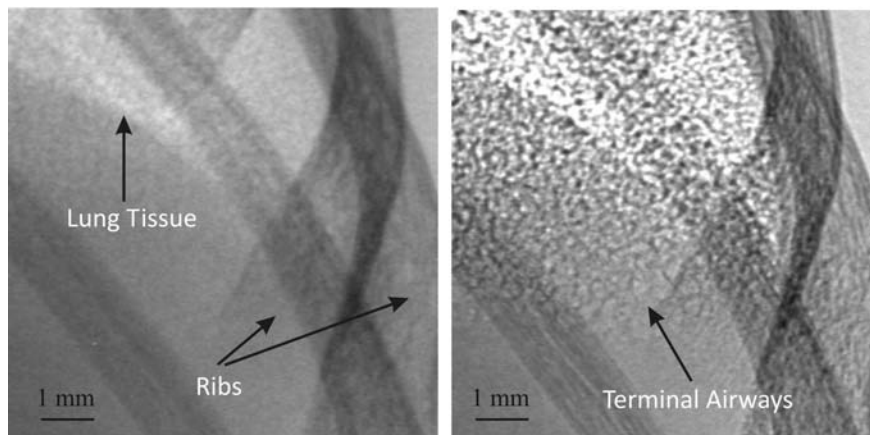


Fig. (3). Images of the lower lobe of a newborn rabbit's thorax imaged with attenuation contrast (*left*) and propagation-based phase contrast (*right*). Phase contrast reveals the terminal airways and a speckled intensity pattern where many airways overlap in projection. Energy: 25 keV. Propagation distances: 5cm (*left*), 1m (*right*).

Fig. (3) compares an absorption contrast X-ray image with a phase contrast image of the chest of a newborn rabbit pup. As can be seen, phase contrast X-ray imaging enhances the boundary contrast between media of dissimilar refractive index (e.g. tissue and bones or air), whilst maintaining an absorption contrast signal. Phase contrast is well suited for imaging lung tissue, which provides only weak absorption contrast due to the small difference in attenuation coefficients at diagnostic X-ray energies. The airways, however, provide sharp interfaces that can be readily seen with phase contrast, enabling even the smallest airways to be observed [60, 62, 65, 66].

Fig. (4) shows a sequence of images recorded at various time points of the first spontaneous breaths of a rabbit pup *in vivo*. This sequence initially shows (a) major airways with (b) further airways becoming visible upon aerated after an additional breath. Image (c) was recorded before the next breath whereby we see some of the airways disappear as fluid flows back along the airways during a period of breathing inactivity. (d)-(h) show further increases in lung aeration after numerous breathing movements. Eventually the major airways become enveloped by a speckled intensity pattern arising from the presence of hundreds of terminal airways becoming aerated [66].

Our recent studies have provided compelling evidence which indicate that lung aeration is closely associated with the pressure gradients generated by inspiration [59-61]. To quantify the relative contribution of inspiration to lung aeration and the creation of an end-expiratory gas volume from birth, phase contrast X-ray imaging has been used simultaneously with plethysmography [61]. Individual breaths accounted for $94.8 \pm 1.4\%$ of the increase in

functional residual capacity (FRC) after birth and only small increases in FRC ($5.2 \pm 1.6\%$) could be detected between breaths (in 15 of 26 pups). Images acquired immediately before and after a single breath Fig. (4) clearly demonstrate the increase in lung aeration associated with a single inspiration, which occurs, on average, at a rate of 9.7 ± 0.8 mL/kg per s (or approximately [35] L/kg per h) over a single breath; breath duration is, on average, approximately 0.3s.

In the experiments just described, measures of lung aeration must equate to airway liquid clearance, otherwise the liquid would remain within the distal airways and coexist with air following lung aeration. For that to occur, the distal airways would need to expand considerably to accommodate both the pre-existing liquid (at least 20 mL/kg [46, 45]) and the increase in air volume (approximately 16 mL/kg) acquired during aeration [61]. With tidal volumes of up to 15 mL/kg immediately after birth, end-inspiratory lung volumes would increase above 50 mL/kg. This would be injurious and force infants to breathe at the top of their pressure-volume curve, thereby decreasing lung compliance with increasing lung aeration. The result would be a thick layer of liquid lining the distal airways, which would greatly increase the barrier for gas diffusion. The potential thickness of this layer can be calculated by approximating the air-filled components of the terminal sacs to be spherical with known radii (approximately $70 \mu\text{m}$ [60]). If no liquid leaves the sacs the terminal sac radius must increase, to accommodate the addition of an equal volume of air, by a factor of 1.26 (to approximately $88 \mu\text{m}$), making the liquid layer approximately $18 \mu\text{m}$ thick. Normally, the thickness of the sac walls is $46 \mu\text{m}$ and the airblood gas barrier is $<1 \mu\text{m}$ for efficient gas exchange. An $18 \mu\text{m}$ thick liquid layer would drastically

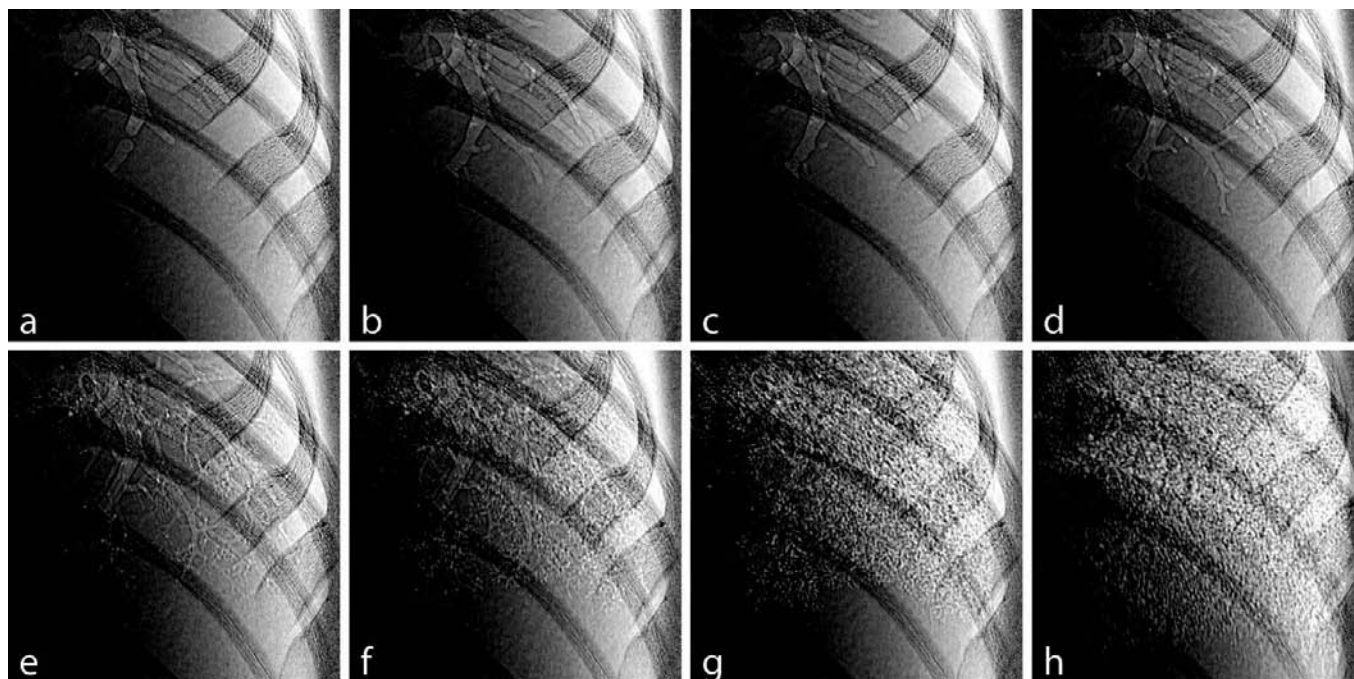


Fig. (4). Propagation-based phase contrast X-ray images of lung aeration at birth using a rabbit pup model. Images were acquired at the SPring-8 synchrotron using 25keV X-rays, an object-to-detector distance of 3m, an exposure time of 588 ms and an interframe time of 4 s. Images were acquired at increments, relative to the first frame, of (a) 0s, (b) 4s, (c) 24s, (d) 28s, (e) 80s, (f) 192s, (g) 320s and (h) 648s. The effective pixel size was $12 \mu\text{m}$. Image size (cropped from images of entire thorax): $5 \text{ mm} \times 5 \text{ mm}$. Image adapted from [60], with permission.

reduce postnatal respiratory function, greatly diminishing the survival rate, and clearly does not normally occur at birth. Furthermore, if liquid was retained within the distal airways, recoil of the expanded airways should force liquid to refill the airways and push the air-liquid interface proximally during expiration [59]. The image sequences (e.g. Fig. (4)) reveal that this is not the case.

Lung liquid can enter the interstitial tissue compartment before eventually being drained via the lymphatic and vascular systems, which can take a number of hours [67]. Because the liquid rapidly (in minutes) leaves the airways during respiration and is cleared from the tissue much more slowly (over hours), the temporary accumulation of water within the interstitial tissue compartment provides an explanation for the known transient (2-4 h) increase in interstitial tissue pressure that occurs immediately after birth. As the water is cleared from lung tissue, the interstitial tissue pressure gradually declines to eventually become subatmospheric (within 6 h), as measured *in situ* in the adult [68]. Furthermore, the combination of liquid retention within the tissue and the increase in airway gas volume can be used to explain the concomitant increase in chest wall expansion that occurs shortly after birth [60].

Lung aeration is evidently associated with inspiration and occurs much more rapidly than is possible via liquid reabsorption, via osmotic gradients generated by Na⁺ reabsorption, alone see Fig. (4). Thus, we have proposed that transepithelial hydrostatic pressures generated by inspiration are the primary driving force for airway liquid clearance after birth [59-61]. This conclusion is backed by the finding that lung aeration also occurs rapidly in deceased ventilated fetal rabbits, in which labour-induced liquid clearance mechanisms, such as adrenaline-induced Na⁺ reabsorption, could not be activated. Because FRC increased and lung compliance decreased with each breath in these dead animals, it appears that hydrostatic pressures can clear airway liquid in the absence of endogenous mechanisms [61].

4. PLATELETS

The primary function of platelets is to maintain haemostasis following vascular injury by adhering to the vessel wall and initiating thrombus formation. Platelet recruitment to the vessel wall also plays a critical role in both chronic and acute phases of cardiovascular diseases, and excessive thrombus formation is directly linked to the resulting ischemic tissue injury and organ dysfunction.

All blood elements in the vascular system experience haemodynamic, or flow induced, forces. The haemodynamic force most relevant to platelet-mediated haemostasis and thrombosis is that generated by shear stress, which is directly related to the local velocity gradient. This can be conceptualised by recognising that the differential in the velocities over the surface of the platelet generates a shearing stress that is felt by the platelet membrane.

Platelet aggregation and subsequent thrombus development is sensitive to both soluble-agonists and haemodynamic forces. The role of soluble-agonists is not covered in this review but is discussed extensively in the

literature, including Ruggeri [69]. A growing body of work has shown that platelet function, including both adhesion and aggregation is dependent on haemodynamic shear. Most early work focused on the effect of bulk shear (within the flow) on the formation of platelet aggregates, which is particularly relevant to circulating platelets passing through cardiovascular prostheses such as artificial heart valves [70]. The majority of these experiments were performed using rotational viscometers, cone-plate or coquette, which expose the entire volume of fluid inside the viscometer to a constant controlled shearing force. The disadvantages of rotational viscometers include that they are difficult to observe, and the shear fields are different from those in real blood vessels. More recently shear experiments have been conducted using parallel flow chambers or channels allowing observation and recording of platelet adhesion and aggregation.

The shear rate (s^{-1}) is commonly used to describe flow conditions, allowing one to avoid the complexities of the viscosity of blood (see Tolouei *et al.* [71] for further information). The shear rate dependence of platelet adhesion and aggregation can be loosely characterised by considering three shear regimes: low shear rate ($<1000s^{-1}$), high shear rate ($1000 - 10000s^{-1}$) and very high (pathological) shear rate ($>10000s^{-1}$) [72]. As the mechanisms of platelet adhesion and aggregation have many of the same pathways, the effect of shear stress on both these mechanisms can be grouped together [73]. At low shear rates platelet are recruited onto collagen, via platelet receptors $\alpha_2\beta_1$ or GPVI, and immobilised von Willebrand factor (vWF) via integrin $\alpha_{IIb}\beta_3$. At higher shear rates platelet adhesion is primarily onto vWF with initial recruitment via GPIb and stabilising recruitment requiring the activation of integrin $\alpha_{IIb}\beta_3$. At pathological shear rates, found in stenosed vessels, adhesion and aggregation occur independently of integrin $\alpha_{IIb}\beta_3$ and activation [74].

During atherosclerosis a considerable quantity of thrombogenic material is stored inside plaques. Consequently, plaque rupture provides an immediate stimulus for platelet adhesion. However, it appears that the flow conditions, generated by the stenosing of the vessel due to plaque development, also play a role. In particular, moyamoya disease causes hyperplasia of smooth-muscle cells in the distal internal carotid artery generating a stenosis without arteriosclerotic or inflammatory changes. This is seen to predispose patients to stroke with pathological analysis showing occlusion of the stenosis with a platelet rich thrombus [75].

Imaging techniques have been extensively used in the investigation of platelet behaviour. Platelets were first described and imaged by Max Schultze [76] in 1865 when he observed platelet aggregations and activated platelets both *in vivo* and *in vitro* [76, 77]. Platelet imaging has revealed much of what is currently known about platelets including shape change during activation, spreading and filopodia formation, adhesion via tether formation and quantitative measures of adhesion and aggregation levels. Fluorescence imaging can also reveal changes in Ca²⁺ flux associated with intracellular changes and is particularly insightful when used in conjunction with imaging of morphological changes [78]. This review now focuses on the use of imaging

techniques to evaluate the effect of shear related forces on platelet adhesion and aggregation.

In order to determine the exact haemodynamic shear force on a platelet the full three-dimensional velocity field around the platelet must be known with at least micron, preferably sub-micron, resolution. An estimate of the shear can be acquired from the two-dimensional plane having the greatest velocity gradients. However, near the vessel wall this is the plane perpendicular to the wall, which unfortunately is the most difficult to measure in the near wall region [79]. Adaption of fluid mechanics techniques such as micro particle image velocimetry (μ PIV) to measure near wall velocity fields in excised blood vessels or chick embryos has shown that poor optical access and near wall distortion limit flow field resolution to the point that useful information at the platelet level is not yet obtainable [80, 81]. Traditional blood flow techniques such as ultrasound, MRI or a combination of ultrasound and PIV algorithms also do not currently offer sufficiently high temporal and spatial resolution [4, 82, 83].

We developed a method combining *in vivo* blood flow experiments and μ PIV [3] over fixed thrombi, revealing the complex nature of the flow fields in regions where platelet aggregations occur. This evidence, combined with observation of platelet behaviour, allowed the formulation of a new model for platelet adhesion and aggregation. Fig. (5a) shows the zones of shear that platelets flowing around and over a thrombi experience. They first experience a low shear (zone 1), followed by a region of high shear (zone 2), followed finally by low shear (zone 3). Platelet adhesion preferentially occurs in the downstream low shear zone (zone 3), with some initial tethering occurring towards the end of the high shear zone (arrows in Fig. (5b)). We concluded that platelet adhesion depends not only on the magnitude of shear but is also sensitive to time varying shear, requiring a period of peak shear followed by a region of shear deceleration. Critically, we found that exposing platelets to a peak shear followed by a shear deceleration caused adhesion even in the absence of soluble agonists. This demonstrated that platelet aggregation is primarily driven by changes in flow induced shearing forces, with soluble agonists having a secondary role by stabilising formed aggregates. Additionally, it has been hypothesised

that it is this shear sequence, peak shear followed by shear deceleration, that causes platelets downstream of mechanical heart valves to activate at a much greater rate (at least 20 times faster) than platelets not initially exposed to high shear [84].

The way in which platelets respond to time varying shear, $\gamma(t)$, appears to be also very sensitive to the magnitude of the upstream wall shear, γ_{pw} . Studies, Colace *et al.* [85] and ourselves [71], have shown that the final geometry of a mature thrombus (no longer growing) depends on γ_{pw} . At lower values of γ_{pw} the thrombi are more circular in shape but as γ_{pw} increases the thrombi become more elongated. We have also shown that at a fixed value of γ_{pw} (1800 s^{-1}) developing thrombi are initially relatively circular but as they develop they become progressively elongated [71]. This is demonstrated by the aggregation sequence shown in Fig. (6) where the majority of platelet aggregation occurs downstream of the initial aggregation point (red cross). While it seems clear that platelets preferentially adhere following a specific sequence of shear stress (high shear followed by low) the fact that mature thrombus geometry depends on the γ_{pw} indicates that platelets respond differently to different $\gamma(t)$ profiles. This is consistent with the extensive body of research that has defined the roles of various platelet receptors with γ_{pw} , however this research now needs to be expanded to consider how these receptors respond to different $\gamma(t)$ profiles.

Combining *in vitro* micro channel imaging with computational fluid dynamics (CFD) simulations can be used to provide detailed information on the $\gamma(t)$ experienced by platelets moving over growing or mature thrombi. In our method the geometry of the thrombi is scanned, reconstructed, meshed and the stresses solved for using three-dimensional CFD. Using this technique we have found that the shear experienced by a thrombus is highly variable, with values varying between zero and up to eight times γ_{pw} .

Whilst platelet response to flow induced shear forces is complex, the fact that cardiovascular diseases have characteristic flow fields not found in the healthy vasculature can be exploited to develop therapies targeted to impede

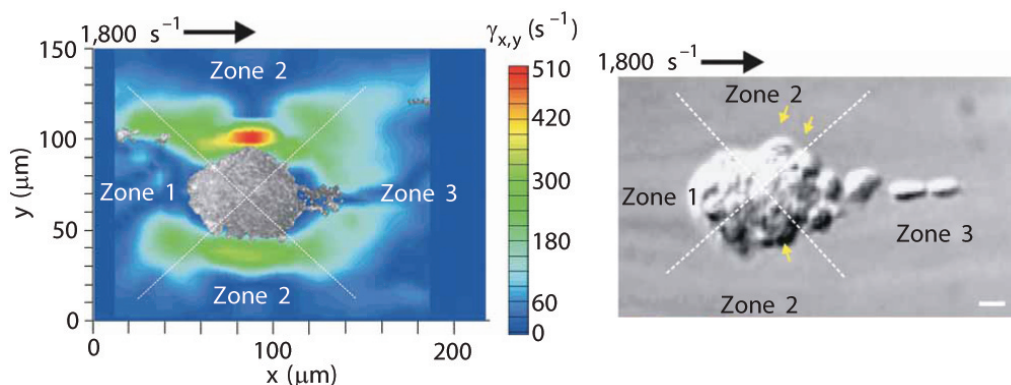


Fig. (5). (a) *In vitro* μ PIV analysis of planar shear rates (γ_{xy}) within $2\mu m$ of the micro-channel floor. (b) Representative differential interference contrast (DIC) image showing discoid platelet tethering to an *in vitro* thrombus at $\gamma_{pw} = 1800 s^{-1}$, yellow arrows show locations of initial platelet recruitment with the majority of stabilised discoid platelet tethering occurring in zone 3 (scale bar, $2\mu m$).

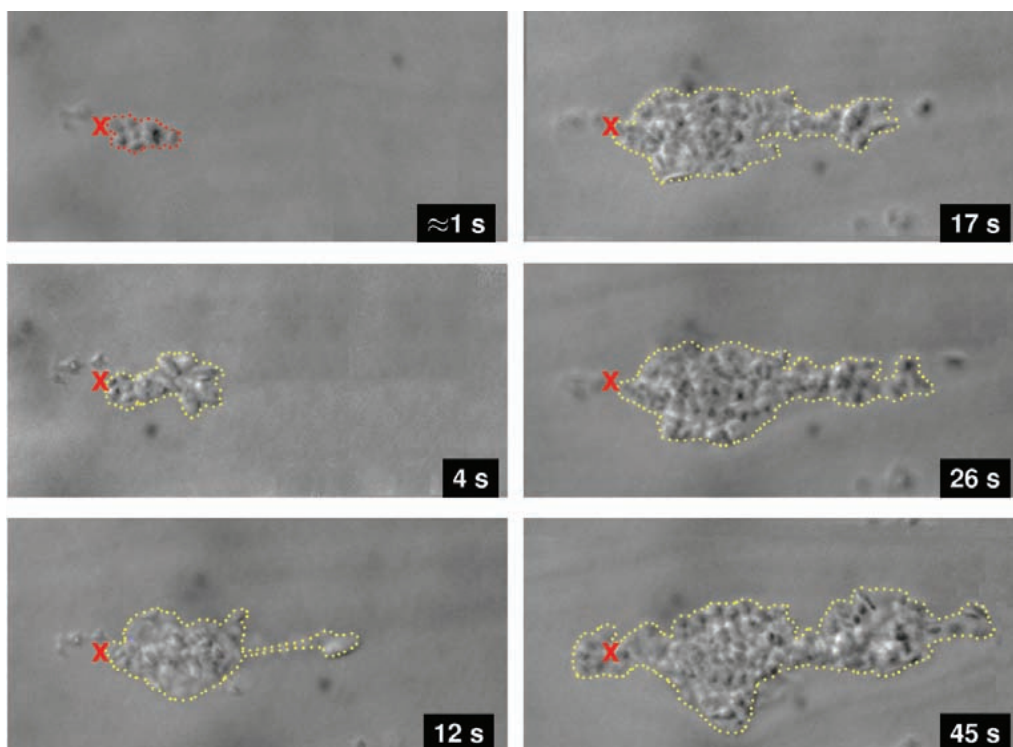


Fig. (6). Bright field microscopy images showing the time-lapsed development of a platelet aggregation. The initial aggregation at $t \approx 1$ s consists of approximately seven platelets indicated by the broken red line. The majority of subsequent recruitment, broken yellow line, occurs downstream of the initial aggregation point marked by a red cross.

pathological thrombus formation. However, more work is required to determine the exact shear sequence experienced by adherent platelets and the corresponding effect on specific platelet receptors.

5. ERYTHROCYTES

The mechanical properties of sub cellular components, in contrast to the mechanical forces experienced by them, are also vital for determining biological function. Of particular interest are the biomechanical properties of the cell membrane as these are subject to manipulation by both dietary intake and in disease. Here we discuss two examples of how sub cellular mechanical properties can alter biological function. The first considers the manner by which cell membrane fluidity in erythrocytes (red blood cells, RBC) alters their ability to flow through blood vessels and the second example assesses the manner by which the fatty acid composition affects the mechanical properties of cell membrane and ultimately the function of cells throughout the body.

Red blood cells, or erythrocytes, are biconcave, non-nucleated cells that are rich in haemoglobin and deliver oxygen throughout the body Fig. (7). Nominally the erythrocyte is approximately $2\text{-}3\mu\text{m}$ in thickness and $7\text{-}10\mu\text{m}$ in diameter, however, these cells must demonstrate a high degree of flexibility in order to travel through the microvasculature of the capillary bed with high efficiency. Indeed, the smallest blood vessels are in the order of $3\text{-}5\mu\text{m}$ in diameter and erythrocytes must deform significantly to pass through these microvessels. Two factors are responsible for erythrocyte flexibility; the lipid content of the cell membrane [86] and the properties of spectrin proteins that

form the protein scaffolding system that lies just below the erythrocyte cell membrane.

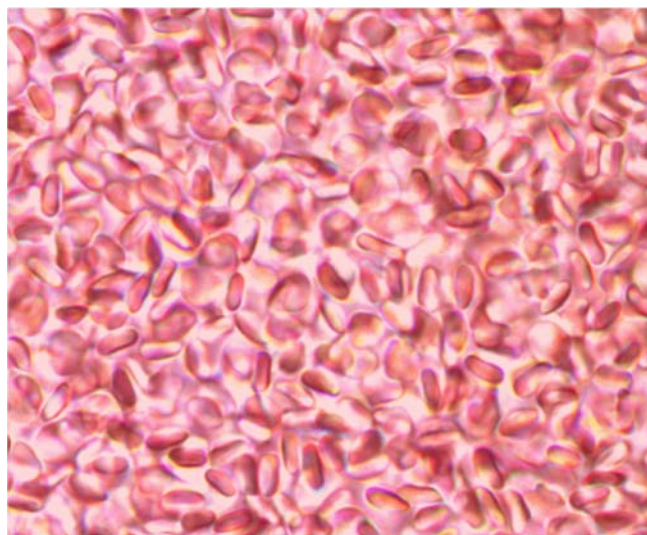


Fig. (7). Photomicrograph of bulk red blood cells (courtesy S. Dubsky and S.C. Irvine).

Alterations in the flexibility or distensibility of erythrocytes have been reported in several diseases including malaria [87] and hypertension [88]. Moreover, computational modelling of erythrocytes also predicts impending diseases such as thalassaemia and anaemia [89]. The distensibility of RBC affects the way these cells flow through small blood vessels and, in diseases such as malaria,

this change in cell distensibility disrupts flow and shear patterns. Altered erythrocyte flexibility is also observed in diabetes [90, 91], a disease that affects over 220 million people worldwide [92].

A range of complications occurs in diabetes, with microvascular disease being implicated in the progression of most of these complications. The accepted pathogenesis in diabetes is that high blood glucose concentration results in an increase in the binding of glucose molecules to proteins (glycosylation). This results in damage to specialised cells in the blood vessel (endothelial cells that line the inside of the vessel and pericytes that form a tight barrier on the outside of small vessels, (see Fig. (1)) and the tissues supplied by these vessels become diseased themselves [93].

There is also evidence to suggest that increased blood viscosity and altered flow dynamics can contribute to diabetic vascular disease [94] and the membrane distensibility of the erythrocyte has been shown to precede vascular disease in diabetics [95]. In fact, even in young diabetic subjects, erythrocyte distensibility is predicted by the level of glycosylation [96] and it is hypothesised that stiffening of erythrocytes is the primary instigating factor in diabetic renal disease [97]. Moreover, recent advances in computational modelling of erythrocytes has lead to prediction of impending disease such as diabetes [89]. There is also evidence that changes in the intracellular environment can change erythrocyte flexibility or distensibility. In diabetes there is a reduction in the concentration of intracellular adenosine triphosphate (ATP). As ATP is the substrate for the activity of sodium potassium exchangers (Na⁺,K⁺-ATPase) this results in an imbalance in intracellular sodium which in turn affects intracellular calcium accumulation and an increase in internal viscosity [98]. Alterations in the makeup of cell membrane lipid content is also important; an increased proportion of saturated fatty acids in membrane phospholipids and cholesterol is seen in diabetes [91, 99] and this can change the biological properties of the cell.

Further work is required to understand why erythrocyte stiffness induces microvascular disease. The haemodynamic view proposed by Zatz and Brenner [100] is compatible with

the notion that stiff erythrocytes do not flow through microvessels efficiently [101], but rather they make repeated contact with the vessel wall, damaging the endothelium, promoting an increase in the permeability of larger blood born proteins and inducing further capillary damage. *In vitro* imaging studies support this hypothesis; stiffer erythrocytes demonstrate increased cell tumbling along the wall of glass microchannels [102]. An alternative hypothesis is that erythrocyte stiffening results in perturbations in flow and this results in increased shear force at the endothelial surface that promotes vascular dysfunction [97] and elevated vessel stiffness which is associated with disease progression [103] (see Section 2 for further endothelial cell discussion).

Characteristic of all cells in animals is the lipid cell membrane that surrounds the cell forming a selective barrier between the intracellular and extracellular environment. A complex array of proteins, receptors, pores and channels are embedded within the cell membrane and these serve to selectively facilitate the transport of nutrients into the cell and waste products from the cell. The correct function of the cell membrane is dependent on a level of structural integrity but excessive stiffness may reduce the functionality of a cell. Here we discuss the manner by which cell membrane biomechanics impact upon the function of diverse cell types in the kidney and liver, neurons in the brain and retina, as well as circulating erythrocytes. However, it is likely that membrane biomechanics affect a range of other biological processes [104-106].

Phospholipids, lipid species comprising a polar phosphatidate headgroup bound to two fatty acids, are the most abundant lipid fraction in animal cell membranes. The type of fat bound to the headgroup is directly proportional to membrane fluidity. Saturated fatty acids pack tightly into a lipid membrane because there is low steric hindrance and high levels of membrane order. This results in a rigid, low fluidity membrane that hinders conformational shape changes in membrane bound proteins and resists membrane deformation [107]. When fatty acids with many double bonds (polyunsaturated fatty acids) are incorporated into the membrane, there is high steric hindrance so phospholipids pack less tightly and the membrane fluidity is greater. Fig. (8) shows this in a simplified fashion. The long chain

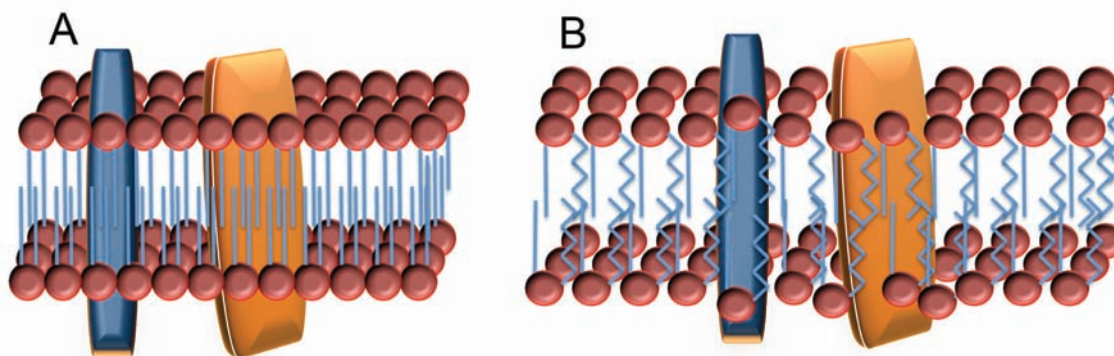


Fig. (8). Cartoon showing two sample phospholipid membranes and receptors. *Left:* the phospholipid membrane is populated with saturated fatty acids. These are low space filling molecules and the membrane packs in an ordered, tight fashion and receptors are held firmly in the membrane. There is resistance to conformational change, hindering receptor activation. *Right:* the phospholipid membrane contains polyunsaturated fatty acids with multiple double bonds and these are highly space filling. As a result the membrane order is low and receptors are held less tightly in this fluid membrane. In this membrane there is minimal mechanical hindrance to receptor conformational change and movement of proteins within the membrane.

omega-3 polyunsaturated fatty acid docosahexaenoic acid (DHA) is the key fatty acid in lipid membranes throughout the central nervous system. Membranes rich in DHA are highly fluid and compressible [108], acting as a molecular spring [109]. This membrane elasticity supports the conformational changes that receptors undergo when they are activated. Indeed, the activity of ion transporters, membrane bound enzymes, G-protein coupled receptors and gene transcription are all affected by membrane biomechanics (see Vingrys *et al.* [105] for review). The rod photoreceptor of the eye is a commonly used model system in which to test the effects of membrane deformability [110] and highly fluid membranes, containing high proportions of DHA, are associated with improved function of these cells [111, 112].

We have demonstrated previously that maternal dietary omega-3 fatty acid intake can result in permanent alterations in the membrane fatty acid composition of the offspring [113, 114]. These changes, a reduction in DHA and an increase in shorter chained fatty acids, are consistent with reduced membrane fluidity. The outcome of this reduction in membrane fatty acid content is hypertension [113, 115], abnormal sodium appetite [116] and a reduction in Na⁺, K⁺ ATPase activity in the kidney, retina and brain [117]. On the other hand, dietary supplementation of DHA results in an improvement in erythrocyte flexibility [86].

Mechanical properties of cells such as erythrocytes can impact directly upon biological processes and the progression of diseases such as diabetes, where a direct mechanical force of erythrocytes at microvessel walls can accelerate the development of vascular disease. Although erythrocyte stiffening precedes diabetic vascular disease, making it potentially a powerful tool in the management of diabetes, to date the relationship between erythrocyte stiffness and disease severity is not often studied. This is owing to the time consuming, non-standardised and highly variable methodology used to assess RBC distensibility. A simple, fast and repeatable method for measuring RBC flexibility is required to exploit the potential of this index of disease progression. A promising technique uses microfluidics [118] to trap cells at a stagnation point which can be used to exert forces on suspended cells, and therefore measure their distensibility. Recent developments in control modelling [119], allow microfluidic systems such as these to be automated, leading to high throughput and repeatability. Moreover, even in non-mobile cells like neurons, the mechanical properties of the cell membrane can modulate the function of receptors to promote disease.

6. CONCLUDING REMARKS

We have examined the previous biochemical approaches for the areas of endothelial cells, lungs, platelets and erythrocytes, and have presented the leading biomechanical theories in four example areas. We have discussed ideas for clinical investigation of arterial disease, providing new insight to our first breaths of life, illuminating the possibility of pharmacological treatments for physically mediated effects and suggesting new diagnostic techniques for diseases such as diabetes. These fields demonstrate the changing outlook for future research, from the biochemical

to the biomechanical, and illustrate that biomechanical effects cannot be neglected. Although we only examine a small section of the biomedical field, we look forward to continued investigation of biomechanical forces, a field that is yet to gain the attention that it requires and deserves.

CONFLICT OF INTEREST

The author(s) confirm that this article content has no conflicts of interest.

ACKNOWLEDGEMENT OF FUNDING

Declared none.

REFERENCES

- King, H.; Aubert, R.; Herman, W. Global burden of diabetes, 1995-2025 - prevalence, numerical estimates, and projections. *Diabetes Care*, **1998**, *21*(9), 1414-1431.
- Sheard, G.J. Flow dynamics and wall shear-stress variation in a fusiform aneurysm. *J. Eng. Math.*, **2009**, *64*(4), 379-390.
- Nesbitt, W.S.; Westein, E.; Tovar-Lopez, F.J.; Tolouei, E.; Mitchell, A.; Fu, J.; Carberry, J.; Fouras, A.; Jackson, S.P. A shear gradient-dependent platelet aggregation mechanism drives thrombus formation. *Nat. Med.*, **2009**, *15*(6), 665-673.
- Fouras, A.; Kitchen, M.J.; Dubsy, S.; Lewis, R.A.; Hooper, S.B.; Hourigan, K. The past, present, and future of x-ray technology for *in vivo* imaging of function and form. *J. Appl. Phys.*, **2009**, *105*(10), 102009.
- Texon, M. The hemodynamic concept of atherosclerosis. *Bull. N.Y. Acad. Med.*, **1960**, *36*(4), 263-274.
- Gimbrone, M. Endothelial dysfunction, hemodynamic forces, and atherosclerosis. *Thromb. Haemostasis*, **1999**, *82*(2), 722-726.
- Flaherty, J.T.; Ferrans, V.J.; Tucker, W.K.; Fry, D.L.; Patel, D.J.; Pierce, J.E. Endothelial nuclear patterns in canine arterial tree with particular reference to hemodynamic events. *Circ. Res.*, **1972**, *30*(1), 23-33.
- Davies, P.F.; Robotewskyj, A.; Griem, M.L. Quantitative studies of endothelial-cell adhesion - directional remodeling of focal adhesion sites in response to flow forces. *J. Clin. Invest.*, **1994**, *93*(5), 2031-2038.
- Ku, D.N.; Giddens, D.P.; Zarins, C.K.; Glagov, S. Pulsatile flow and atherosclerosis in the human carotid bifurcation - positive correlation between plaque location and low and oscillating shear-stress. *Arteriosclerosis*, **1985**, *5*(3), 293-302.
- Chatzizisis, Y.S.; Coskun, A.U.; Jonas, M.; Edelman, E.R.; Feldman, C.L.; Stone, P.H. Role of endothelial shear stress in the natural history of coronary atherosclerosis and vascular remodeling: molecular, cellular, and vascular behavior. *J. Am. Coll. Cardiol.*, **2007**, *49*(25), 2379-2393.
- Feldman, C.; Ilegbusi, O.; Hu, Z.; Nesto, R.; Waxman, S.; Stone, P. Determination of *in vivo* velocity and endothelial shear stress patterns with phasic flow in human coronary arteries: A methodology to predict progression of coronary atherosclerosis. *Am. Heart J.*, **2002**, *143*(6), 931-939.
- Baek, H.; Jayaraman, M.V.; Karniadakis, G.E. Wall shear stress and pressure distribution on aneurysms and infundibulae in the posterior communicating artery bifurcation. *Ann. Biomed. Eng.*, **2009**, *37*(12), 2469-2487.
- Jamison, R.A.; Dubsy, S.; Siu, K.K.W.; Hourigan, K.; Fouras, A. X-ray velocimetry and haemodynamic forces within a stenosed femoral model at physiological flow rates. *Ann. Biomed. Eng.*, **2011**, *39*(6), 1643-1653.
- Shojima, M.; Oshima, M.; Takagi, K.; Torii, R.; Hayakawa, M.; Katada, K.; Morita, A.; Kirino, T. Magnitude and role of wall shear stress on cerebral aneurysm: Computational fluid dynamic study of 20 middle cerebral artery aneurysms. *Stroke*, **2004**, *35*(11), 2500-2505.
- Cheng, C. Atherosclerotic lesion size and vulnerability are determined by patterns of fluid shear stress. *Circulation*, **2006**, *113*(23), 2744-2753.

- [16] Conklin, B.; Zhong, D.; Zhao, W.; Lin, P.; Chen, C. Shear stress regulates occludin and VEGF expression in porcine arterial endothelial cells. *J. Surg. Res.*, **2002**, *102*(1), 13-21.
- [17] Gertz, S.D.; Roberts, W.C. Hemodynamic shear force in rupture of coronary arterial atherosclerotic plaques. *Am. J. Cardiol.*, **1990**, *66*(19), 1368-1372.
- [18] Resnick, N.; Yahav, H.; Shay-Salit, A.; Shushy, M.; Schubert, S.; Zilberman, L.; Wofovitz, E. Fluid shear stress and the vascular endothelium: for better and for worse. *Prog. Biophys. Mol. Biol.*, **2003**, *81*(3), 177-199.
- [19] Guyton, J.; Klemp, K. Development of the lipid-rich core in human atherosclerosis. *Arterioscl. Throm. Vasc.*, **1996**, *16*(1), 4-11.
- [20] Caro, C.G.; Fitz-Gerald, J.M.; Schroter, R.C. Arterial wall shear and distribution of early atheroma in man. *Nature*, **1969**, *223*(5211), 1159-1161.
- [21] Malek, A.; Alper, S.; Izumo, S. Hemodynamic shear stress and its role in atherosclerosis. *JAMA*, **1999**, *282*(21), 2035.
- [22] Glagov, S.; Weisenberg, E.; Zarins, C.K.; Stankunavicius, R.; Kolettis, G.J. Compensatory enlargement of human atherosclerotic coronary-arteries. *N. Engl. J. Med.*, **1987**, *316*(22), 1371-1375.
- [23] Stone, P.H.; Coskun, A.U.; Kinlay, S.; Popma, J.J.; Sonka, M.; Wahle, A.; Yeghiazarians, Y.; Maynard, C.; Kuntz, R.E.; Feldman, C.L. Regions of low endothelial shear stress are the sites where coronary plaque progresses and vascular remodeling occurs in humans: an *in vivo* serial study. *Eur. Heart J.*, **2007**, *28*(6), 705-710.
- [24] Birnbaum, Y.; Fishbein, M.; Luo, H.; Nishioka, T.; Siegel, R. Regional remodeling of atherosclerotic arteries: A major determinant of clinical manifestations of disease. *J. Am. Coll. Cardiol.*, **1997**, *30*(5), 1149-1164.
- [25] Feldman, C.; Stone, P. Intravascular hemodynamic factors responsible for progression of coronary atherosclerosis and development of vulnerable plaque. *Curr. Opin. Cardiol.*, **2000**, *15*(6), 430-440.
- [26] Fry, D.L. Acute vascular endothelial changes associated with increased blood velocity gradients. *Circ. Res.*, **1968**, *22*(2), 165-197.
- [27] Leuprecht, A.; Perktold, K.; Kozerke, S.; Boesiger, P. Combined CFD and MRI study of blood flow in a human ascending aorta model. *Biorheology*, **2002**, *39*(3-4), 425-429.
- [28] Oshima, M.; Torii, R.; Tokuda, S.; Yamada, S.; Koizumi, A. Patient-specific modeling and multi-scale blood simulation for computational hemodynamic study on the human cerebrovascular system. *Curr. Pharm. Biotechnol.*, **2012**, *13*(11), ???-???
- [29] August, A.D.; Barratt, D.C.; Hughes, A.D.; Glor, F.P.; Thom, S.A.M.; Xu, X.Y. Accuracy and reproducibility of CFD predicted wall shear stress using 3D ultrasound images. *J. Biomech. Eng-T Asme*, **2003**, *125*(2), 218-222.
- [30] Moyle, K.R.; Antiga, L.; Steinman, D.A. Inlet conditions for image-based CFD models of the carotid bifurcation: Is it reasonable to assume fully developed flow?. *J. Biomech. Eng-T Asme*, **2006**, *128*(3), 371-379.
- [31] Ford, M.D.; Nikolov, H.N.; Milner, J.S.; Lownie, S.P.; DeMont, E.M.; Kalata, W.; Loth, F.; Holdsworth, D.W.; Steinman, D.A. PIV-measured versus CFD-predicted flow dynamics in anatomically realistic cerebral aneurysm models. *J. Biomech. Eng-T Asme*, **2008**, *130*(2), 021015.
- [32] Hoi, Y.; Woodward, S.H.; Kim, M.; Taulbee, D.B.; Meng, H. Validation of CFD simulations of cerebral aneurysms with implication of geometric variations. *J. Biomech. Eng-T Asme*, **2006**, *128*(6), 844-851.
- [33] Dubsy, S.; Jamison, R.A.; Irvine, S.C.; Siu, K.K.W.; Hourigan, K.; Fouras, A. Computed tomographic x-ray velocimetry. *Appl. Phys. Lett.*, **2010**, *96*(2), 023702.
- [34] Irvine, S.C.; Paganin, D.M.; Jamison, A.; Dubsy, S.; Fouras, A. Vector tomographic x-ray phase contrast velocimetry utilizing dynamic blood speckle. *Opt. Express*, **2010**, *18*(3), 2368-2379.
- [35] Lee, S.J.; Kim, G.B. Synchrotron microimaging technique for measuring the velocity fields of real blood flows. *J. Appl. Phys.*, **2005**, *97*(6), 064701.
- [36] Fouras, A.; Dusting, J.; Lewis, R.; Hourigan, K. Three-dimensional synchrotron x-ray particle image velocimetry. *J. Appl. Phys.*, **2007**, *102*(6), 064916.
- [37] Irvine, S.C.; Paganin, D.M.; Dubsy, S.; Lewis, R.A.; Fouras, A. Phase retrieval for improved three-dimensional velocimetry of dynamic x-ray blood speckle. *Appl. Phys. Lett.*, **2008**, *93*(15), 153901.
- [38] Fouras, A.; Soria, J. Accuracy of out-of-plane vorticity measurements derived from in-plane velocity field data. *Exp. Fluids.*, **1998**, *25*(5-6), 409-430.
- [39] Dubsy, S.; Jamison, R.A.; Higgins, S.P.A.; Siu, K.K.W.; Hourigan, K.; Fouras, A. Computed tomographic x-ray velocimetry for simultaneous 3D measurement of velocity and geometry in opaque vessels. *Exp. Fluids*, **2011**, *52*(3), 543-554. DOI 10.1007/s00348-010-1006-x.
- [40] Hogg, J. Pathophysiology of airflow limitation in chronic obstructive pulmonary disease. *Lancet*, **2004**, *364*(9435), 709-721.
- [41] Sethi, S.; Murphy, T.F. Current concepts: Infection in the pathogenesis and course of chronic obstructive pulmonary disease. *N. Engl. J. Med.*, **2008**, *359*(22), 2355-2365.
- [42] Allen, G.; Pavone, L.; DiRocco, J.; Bates, J.; Nieman, G. Pulmonary impedance and alveolar instability during injurious ventilation in rats. *J. Appl. Physiol.*, **2005**, *99*(2), 723-730.
- [43] Black, C.L.B.; Hoffman, A.M.; Tsai, L.W.; Ingenito, E.P.; Suki, B.; Kaczka, D.W.; Simon, B.A.; Lutchen, K.R. Relationship between dynamic respiratory mechanics and disease heterogeneity in sheep lavage injury. *Crit. Care Med.*, **2007**, *35*(3), 870-878.
- [44] Boulet, L.P.; Belanger, M.; Carrier, G. Airway responsiveness and bronchial-wall thickness in asthma with or without fixed air-flow obstruction. *Am. J. Resp. Crit. Care*, **1995**, *152*(3), 865-871.
- [45] Harding, R.; Hooper, S.B. Regulation of lung expansion and lung growth before birth. *J. Appl. Physiol.*, **1996**, *81*(1), 209-224.
- [46] Hooper, S.B.; Harding, R. Fetal lung liquid: a major determinant of the growth and functional development of the fetal lung. *Clin. Exp. Pharmacol. Physiol.*, **1995**, *22*(4), 235-247.
- [47] Jain, L.; Eaton, D.C. Physiology of fetal lung fluid clearance and the effect of labor. *Semin. Perinatol.*, **2006**, *30*(1), 34-43.
- [48] Olver, R.E.; Walters, D.V.; Wilson, S.M. Developmental regulation of lung liquid transport. *Annu. Rev. Physiol.*, **2004**, *66*, 77-101.
- [49] te Pas, A.B.; Davis, P.G.; Hooper, S.B.; Morley, C.J. From liquid to air: breathing after birth. *J. Pediatr.*, **2008**, *152*(5), 607-611.
- [50] Hooper, S.B.; Harding, R. Effect of beta-adrenergic blockade on lung liquid secretion during fetal asphyxia. *Am. J. Physiol.*, **1989**, *257*(4 Pt 2), R705-710.
- [51] Olver, R.E.; Ramsden, C.A.; Strang, L.B.; Walters, D.V. The role of amiloride-blockable sodium transport in adrenaline-induced lung liquid reabsorption in the fetal lamb. *J. Physiol (Lond)*, **1986**, *376*, 321-340.
- [52] Walters, D.V.; Olver, R.E. The role of catecholamines in lung liquid absorption at birth. *Pediatr. Res.*, **1978**, *12*(3), 239-242.
- [53] Wallace, M.J.; Hooper, S.B.; Harding, R. Role of the adrenal glands in the maturation of lung liquid secretory mechanisms in fetal sheep. *Am. J. Physiol.*, **1996**, *270*(1 Pt 2), R33-40.
- [54] Vyas, H.; Milner, A.D.; Hopkins, I.E. Intrathoracic pressure and volume changes during the spontaneous onset of respiration in babies born by cesarean section and by vaginal delivery. *J. Pediatr.*, **1981**, *99*(5), 787-791.
- [55] Bland, R.D. Loss of liquid from the lung lumen in labor: more than a simple "squeeze". *Am. J. Physiol. Lung. Cell Mol. Physiol.*, **2001**, *280*(4), L602-605.
- [56] Harding, R.; Hooper, S.B.; Dickson, K.A. A mechanism leading to reduced lung expansion and lung hypoplasia in fetal sheep during oligohydramnios. *Am. J. Obstet. Gynecol.*, **1990**, *163*(6 Pt 1), 1904-1913.
- [57] Dickson, K.A.; Harding, R. Compliances of the liquid-filled lungs and chest wall during development in fetal sheep. *J. Dev. Physiol.*, **1991**, *16*(2), 105-113.
- [58] Lines, A.; Hooper, S.B.; Harding, R. Lung liquid production rates and volumes do not decrease before labor in healthy fetal sheep. *J. Appl. Physiol.*, **1997**, *82*(3), 927-932.
- [59] Hooper, S.B.; Kitchen, M.J.; Siew, M.L.L.; Lewis, R.A.; Fouras, A.; Pas, teA.B.; Siu, K.K.W.; Yagi, N.; Uesugi, K.; Wallace, M.J. Imaging lung aeration and lung liquid clearance at birth using phase contrast x-ray imaging. *Clin. Exp. Pharm. Physiol.*, **2009**, *36*(1), 117-125.
- [60] Hooper, S.B.; Kitchen, M.J.; Wallace, M.J.; Yagi, N.; Uesugi, K.; Morgan, M.J.; Hall, C.; Siu, K.K.W.; Williams, I.M.; Siew, M.; Irvine, S.C.; Pavlov, K.; Lewis, R.A. Imaging lung aeration and lung liquid clearance at birth. *FASEB J.*, **2007**, *21*(12), 3329-3337.
- [61] Siew, M.L.; Wallace, M.J.; Kitchen, M.J.; Lewis, R.A.; Fouras, A.; Pas, teA.B.; Yagi, N.; Uesugi, K.; Siu, K.K.W.; Hooper, S.B. Inspiration regulates the rate and temporal pattern of lung liquid

- clearance and lung aeration at birth. *J. Appl. Physiol.*, **2009**, *106*(6), 1888-1895.
- [62] Kitchen, M.J.; Lewis, R.A.; Yagi, N.; Uesugi, K.; Paganin, D.; Hooper, S.B.; Adams, G.; Jureczek, S.; Singh, J.; Christensen, C.R.; Hufton, A.P.; Hall, C.J.; Cheung, K.C.; Pavlov, K.M. Phase contrast x-ray imaging of mice and rabbit lungs: a comparative study. *Br. J. Radiol.*, **2005**, *78*(935), 1018-1027.
- [63] Nugent, K.A. Coherent methods in the x-ray sciences. *Adv. Phys.*, **2010**, *59*(1), 1-99.
- [64] Snigireva, A.; Snigireva, I.; Kohn, V.; Kuznetsov, S.; Schelokov, I. On the possibilities of x-ray phase contrast microimaging by coherent high-energy synchrotron radiation. *Rev. Scientific Instrum.*, **1995**, *66*(12), 5486-5492.
- [65] Lewis, R.A.; Yagi, N.; Kitchen, M.J.; Morgan, M.J.; Paganin, D.; Siu, K.K.W.; Pavlov, K.; Williams, I.; Uesugi, K.; Wallace, M.J.; Hall, C.J.; Whitley, J.; Hooper, S.B. Dynamic imaging of the lungs using x-ray phase contrast. *Phys. Med. Biol.*, **2005**, *50*(21), 5031-5040.
- [66] Kitchen, M.J.; Paganin, D.; Lewis, R.A.; Yagi, N.; Uesugi, K.; Mudie, S.T. On the origin of speckle in x-ray phase contrast images of lung tissue. *Phys. Med. Biol.*, **2004**, *49*(18), 4335-4348.
- [67] Bland, R.D.; McMillan, D.D.; Bressack, M.A.; Dong, L. Clearance of liquid from lungs of newborn rabbits. *J. Appl. Physiol.*, **1980**, *49*(2), 171-177.
- [68] Miserocchi, G.; Poskurica, B.H.; Fabbro, M.D. Pulmonary interstitial pressure in anesthetized paralyzed newborn rabbits. *J. Appl. Physiol.*, **1994**, *77*(5), 2260-2268.
- [69] Ruggeri, Z.M. Platelets in atherothrombosis. *Nat. Med.*, **2002**, *8*(11), 1227-1234.
- [70] Brown, C.H.; Leverett, L.B.; Lewis, C.W.; Alfrey, C.P.; Hellums, J.D. Morphological, biochemical, and functional changes in human platelets subjected to shear stress. *J. Lab. Clin. Med.*, **1975**, *86*(3), 462-471.
- [71] Tolouei, E.; Butler, C.J.; Fouras, A.; Ryan, K.; Sheard, G.J.; Carberry, J. Effect of hemodynamic forces on platelet aggregation geometry. *Ann. Biomed. Eng.*, **2011**, *39*(5), 1403-1413.
- [72] Maxwell, M.J.; Westein, E.; Nesbitt, W.S.; Giuliano, S.; Dopheide, S.M.; Jackson, S.P. Identification of a 2-stage platelet aggregation process mediating shear-dependent thrombus formation. *Blood*, **2007**, *109*(2), 566-576.
- [73] Ruggeri, Z.M.; Mendolicchio, G.L. Adhesion mechanisms in platelet function. *Circ. Res.*, **2007**, *100*(12), 1673-1685.
- [74] Jackson, S.P. The growing complexity of platelet aggregation. *Blood*, **2007**, *109*(12), 5087-5095.
- [75] Scott, R.M.; Smith, E.R. Moyamoya disease and moyamoya syndrome. *N. Engl. J. Med.*, **2009**, *360*(12), 1226-1237.
- [76] Schultze, M. Ein heizbarer objectisch und seine verwendung bei untersuchungen des blutes. *Archiv für mikroskopische Anatomie*, **1865**.
- [77] Brewer, D.B.; Schultze, M (1865), Bizzozero G. (1882) and the discovery of the platelet. *Br. J. Haematol.*, **2006**, *133*(3), 251-258.
- [78] Ikeda, M.; Ariyoshi, H.; Kambayashi, J.; Sakon, M.; Kawasaki, T.; Monden, M. Simultaneous digital imaging analysis of cytosolic calcium and morphological change in platelets activated by surface contact. *J. Cell Biochem.*, **1996**, *61*(2), 292-300.
- [79] Nguyen, C.V.; Fouras, A.; Carberry, J. Improvement of measurement accuracy in micro PIV by image overlapping. *Exp. Fluids*, **2010**, *49*(3), 701-712.
- [80] Sugii, Y.; Nishio, S.; Okamoto, K. *In vivo* PIV measurement of red blood cell velocity field in microvessels considering mesentery motion. *Physiol. Meas.*, **2002**, *23*(2), 403-416.
- [81] Vennemann, P.; Kiger, K.T.; Lindken, R.; Groenendijk, B.C.W.; Vos, deS.S.; Hagen, tenT.L.M.; Ursem, N.T.C.; Poelmann, R.E.; Westerweel, J.; Hierck, B.P. *In vivo* micro particle image velocimetry measurements of blood-plasma in the embryonic avian heart. *J. Biomech.*, **2006**, *39*(7), 1191-1200.
- [82] Nam, K.-H.; Yeom, E.; Ha, H.; Lee, S.-J. Velocity field measurements of valvular blood flow in a human superficial vein using high-frequency ultrasound speckle image velocimetry. *Intl. J. Cardiovasc. Imaging*, **2010**, [Epub ahead of print]
- [83] Qian, M.; Niu, L.; Wang, Y.; Jiang, B.; Jin, Q.; Jiang, C.; Zheng, H. Measurement of flow velocity fields in small vessel-mimic phantoms and vessels of small animals using micro ultrasonic particle image velocimetry (micro-EPIV). *Physics Med. Biol.*, **2010**, *55*(20), 6069-6088.
- [84] Sheriff, J.; Bluestein, D.; Girdhar, G.; Jesty, J. High-shear stress sensitizes platelets to subsequent low-shear conditions. *Ann. Biomed. Eng.*, **2010**, *38*(4), 1442-1450.
- [85] Colace, T.; Falls, E.; Zheng, X.L.; Diamond, S.L. Analysis of morphology of platelet aggregates formed on collagen under laminar blood flow. *Ann. Biomed. Eng.*, **2011**, *39*(2), 922-929.
- [86] Popp-Snijders, C.; Schouten, J.A.; Blitterswijk, vanW.J.; Veen, van derE.A. Changes in membrane lipid composition of human erythrocytes after dietary supplementation of (n-3) polyunsaturated fatty acids. maintenance of membrane fluidity. *Biochim. Biophys. Acta*, **1986**, *854*(1), 31-37.
- [87] Pistea, A.; Bakker, E.N. T.P.; Spaan, J.A.E.; Hardeman, M.R.; Rooijen, vanN.; VanBavel, E. Small artery remodeling and erythrocyte deformability in l-name-induced hypertension: role of transglutaminases. *J. Vasc. Res.*, **2008**, *45*(1), 10-18.
- [88] Roggenkamp, H.G.; Jung, F.; Nüttgens, H.P.; Kiesewetter, H.; Ringelstein, E.B.; Schneider, R. Erythrocyte rigidity in healthy patients and patients with cardiovascular disease risk factors. *Klin Wochenschr*, **1986**, *64*(20), 1091-1096.
- [89] Weatherall, D.J. Systems biology and red cells. *N. Engl. J. Med.*, **2011**, *364*(4), 376-377.
- [90] Babu, N.; Singh, M. Influence of hyperglycemia on aggregation, deformability and shape parameters of erythrocytes. *Clin. Hemorheol. Micro*, **2004**, *31*(4), 273-280.
- [91] Garnier, M.; Attali, J.R.; Valensi, P.; Delatour-Hanss, E.; Gaudy, F.; Koutsouris, D. Erythrocyte deformability in diabetes and erythrocyte membrane lipid composition. *Metab. Clin. Exp.*, **1990**, *39*(8), 794-798.
- [92] Wild, S.; Roglic, G.; Green, A.; Sicree, R.; King, H. Global prevalence of diabetes: estimates for the year 2000 and projections for 2030. *Diabetes Care*, **2004**, *27*(5), 1047-1053.
- [93] Rahman, S.; Rahman, T.; Ismail, A.A.-S.; Rashid, A.R.A. Diabetes-associated macrovasculopathy: pathophysiology and pathogenesis. *Diabetes Obes. Metab.*, **2007**, *9*(6), 767-780.
- [94] Kiesewetter, H.; Jung, F. Blood fluidity and endothelial influences on microcirculation. *J. Mol. Med.*, **1986**, *64*(19), 943-992.
- [95] Diamantopoulos, E.J.; Kittas, C.; Charitos, D.; Grigoriadou, M.; Ifanti, G.; Raptis, S.A. Impaired erythrocyte deformability precedes vascular changes in experimental diabetes mellitus. *Horm. Metab. Res.*, **2004**, *36*(3), 142-147.
- [96] Tillmann, W.; Merten, A.; Lakomek, M.; Gahr, M.; Fiechtl, J.; Schröter, W. Flexibility of erythrocytes in juvenile diabetes mellitus. *Blut*, **1981**, *43*(2), 125-8.
- [97] Simpson, L.O. Intrinsic stiffening of red blood cells as the fundamental cause of diabetic nephropathy and microangiopathy: a new hypothesis. *Nephron*, **1985**, *39*(4), 344-351.
- [98] Vague, P.; Coste, T.C.; Jannot, M.F.; Raccach, D.; Tsimaratos, M. C-peptide, Na⁺-K⁺-ATPase, and diabetes. *Exp. Diabetes Res.*, **2004**, *5*(1), 37-50.
- [99] Plasenzotti, R.; Windberger, U.; Ulberth, F.; Osterode, W.; Losert, U. Influence of fatty acid composition in mammalian erythrocytes on cellular aggregation. *Clin. Hemorheol. Micro*, **2007**, *37*(3), 237-43.
- [100] Zatz, R.; Brenner, B.M. Pathogenesis of diabetic microangiopathy. the hemodynamic view. *Am. J. Med.*, **1986**, *80*(3), 443-453.
- [101] Shin, S.; Ku, Y.; Babu, N.; Singh, M. Erythrocyte deformability and its variation in diabetes mellitus. *Indian J. Exp. Biol.*, **2007**, *45*(1), 121-128.
- [102] Forsyth, A.M.; Wan, J.; Ristenpart, W.D.; Stone, H.A. The dynamic behavior of chemically "stiffened" red blood cells in microchannel flows. *Microvasc. Res.*, **2010**, *80*(1), 37-43.
- [103] Lee, S.S.; Kim, N.J.; Sun, K.; Dobbe, J.G.; Hardeman, M.R.; Antaki, J.F.; Ahn, K.H.; Lee, S.J. Association between arterial stiffness and the deformability of red blood cells (RBCs). *Clin. Hemorheol. Micro*, **2006**, *34*(4), 475-481.
- [104] Litman, B.J.; Mitchell, D.C. A role for phospholipid polyunsaturation in modulating membrane protein function. *Lipids*, **1996**, *31*, S193-197.
- [105] Vingrys, A.; Armitage, J.; Weisinger, H.S.; Bui, B.V.; Sinclair, A.J.; Weisinger, R.S. In: *The Role of omega-3 polyunsaturated fatty acids in retinal function*. Humana Press Totowa, NJ, **2001**, 193-217.
- [106] Weisinger, H.; Armitage, J.; Jeffrey, B.; Mitchell, D.; Moriguchi, T.; Sinclair, A.; Weisinger, R.; Salem, N. Retinal sensitivity loss in third-generation n-3 pufa-deficient rats. *Lipids*, **2002**, *37*(8), 759-765.

- [107] Litman, B.; Mitchell, D. A role for phospholipid polyunsaturation in modulating membrane protein function. *Lipids*, **1996**, *31*, S193-S197.
- [108] Huber, T.; Rajamoorthi, K.; Kurze, V.F.; Beyer, K.; Brown, M.F. Structure of docosahexaenoic acid-containing phospholipid bilayers as studied by $(2)H$ NMR and molecular dynamics simulations. *J. Am. Chem. Soc.*, **2002**, *124*(2), 298-309.
- [109] Holte, L.L.; Dratz, E.A. The molecular spring model for docosahexaenoic acid function in biological-membranes. *Biophys. J.*, **1993**, *64*(2), A289-A289.
- [110] Niu, S.-L.; Mitchell, D.C.; Lim, S.-Y.; Wen, Z.-M.; Kim, H.-Y.; Salem, N.; Litman, B.J. Reduced G protein-coupled signaling efficiency in retinal rod outer segments in response to n-3 fatty acid deficiency. *J. Biol. Chem.*, **2004**, *279*(30), 31098-31104.
- [111] Benolken, R.M.; Anderson, R.E.; Wheeler, T.G. Membrane fatty acids associated with the electrical response in visual excitation. *Science*, **1973**, *182*(118), 1253-1254.
- [112] Weisinger, H.S.; Armitage, J.A.; Jeffrey, B.G.; Mitchell, D.C.; Moriguchi, T.; Sinclair, A.J.; Weisinger, R.S.; Salem, N. Retinal sensitivity loss in third-generation n-3 pufa-deficient rats. *Lipids*, **2002**, *37*(8), 759-765.
- [113] Armitage, J.A.; Pearce, A.D.; Sinclair, A.J.; Vingrys, A.J.; Weisinger, R.S.; Weisinger, H.S. Increased blood pressure later in life may be associated with perinatal n-3 fatty acid deficiency. *Lipids*, **2003**, *38*(4), 459-464.
- [114] Li, D.; Weisinger, H.S.; Weisinger, R.S.; Mathai, M.; Armitage, J.A.; Vingrys, A.J.; Sinclair, A.J. Omega 6 to omega 3 fatty acid imbalance early in life leads to persistent reductions in DHA levels in glycerophospholipids in rat hypothalamus even after long-term omega 3 fatty acid repletion. *Prostaglandins Leukot Essent Fatty Acids*, **2006**, *74*(6), 391-399.
- [115] Weisinger, H.; Armitage, J.; Sinclair, A.; Vingrys, A.; Burns, P.; Weisinger, R. Perinatal omega-3 fatty acid deficiency affects blood pressure later in life. *Nat. Med.*, **2001**, *7*(3), 258-259.
- [116] Weisinger, R.S.; Armitage, J.A.; Chen, N.; Begg, D.P.; Mathai, M.L.; Jayasooriya, A.P.; Sinclair, A.J.; Weisinger, H.S. Sodium appetite in adult rats following ω -3 polyunsaturated fatty acid deficiency in early development. *Appetite*, **2010**, *55*(3), 393-397.
- [117] Armitage, J.A.; Gupta, S.; Wood, C.; Jensen, R.I.; Samuelsson, A.-M.; Fuller, W.; Shattock, M.J.; Poston, L.; Taylor, P.D. Maternal dietary supplementation with saturated, but not monounsaturated or polyunsaturated fatty acids, leads to tissue-specific inhibition of offspring Na^+ , K^+ ATPase. *J. Physiol (Lond)*, **2008**, *586*(Pt 20), 5013-5022.
- [118] Tanyeri, M.; Johnson-Chavarria, E.M.; Schroeder, C.M. Hydrodynamic trap for single particles and cells. *Appl. Phys. Lett.*, **2010**, *96*(22), 224101.
- [119] Curtis, M.D.; Sheard, G.J.; Fouras, A. Feedback control system simulator for the control of biological cells in microfluidic cross slots and integrated microfluidic systems. *Lab. Chip*, **2011**, *11*(14), 2343-2351.